NPS-57FU8101A

UNITED STATES
NAVAL POSTGRADUATE SCHOOL

AERONAUTICAL APPLICATIONS OF HOLOGRAPHIC INTERFEROMETRY

by

R. D. Matulka
J. H. Holds
J. G. Sullivan
A. E. Fuhs

NAVAL POSTGRADUATE SCHOOL
Monterey, California

Rear Admiral R. W. McNitt, USN
Superintendent

R. F. Rinehart
Academic Dean

ABSTRACT:

The use of holography for the production of wind-tunnel interferograms of the Mach-Zehnder type is described with a discussion of the possibility of extending the process toward the interferometric study of three-dimensional flow fields. Two initial studies toward an understanding of the processes involved in three-dimensional interferometric reduction are described: (1) the hologram as a diffraction grating, and (2) intensity variation beyond both a hologram and a diffuse glass plate. Lastly, a complete prediction of a hologram of a simple, two dimensional, aperture is made. This prediction provides a tutorial device for the understanding of holography of the type used in holographic interferometry.

NPS-57FU8101A

LIST OF ILLUSTRATIONS

I. INTRODUCTION

Development of Holography

In 1948 Dennis Gabor reported a new principle for microscopy in which the actual wavefront of emanating light rays is captured on film by means of a diffraction pattern.[1] The motivation for Gabor's research was to increase the resolution of electron microscopes. For these diffraction patterns on film, he later coined the term "Hologram."[2] Gabor's method proved to be applicable to many fields other than microscopy, but was limited by its requirement for highly monocromatic light.

The first laser was achieved in 1960. Its monochromaticity, temporal and spacial coherence, and uniform collimation, by providing an ideal source of light, have spurred a very rapid growth in the science of wavefront reconstruction, or holography. For an excellent general description of the holographic process, the reader is referred to articles by Leith and Upatnieks[3], Pennington[4], and Brandt.[5] Holography is dealt with in depth in many technical papers, notably those by Leith and Upatnieks[6], and in books by Develis and Reynolds[7] and by Stroke.[8] An excellent bibliography of the subject has been compiled by Chambers and Courtney-Pratt.[9]

Application of Holography to Aeronautics

Among the developing applications of holography, of interest to the aeronautical engineer, is interferometry. This paper deals with recent activities in this field at the Department of Aeronautics of the Naval Postgraduate School. First holographic interferometry and the holographic

interferometer in use at NPGS are discussed.

One of the peculiar capabilities of this method is the ability to produce three-dimensional interferograms of the flow about models. The correlation between the density field about the model and the phase and amplitude of the resulting intensity pattern remains an unsolved problem. Section III discusses some work conducted at NPGS towards an understanding of this problem; these studies include:

(1) A comparison of the properties of a dark-field hologram with those of a lined diffraction grating.

(2) An experimental examination of the intensity patterns from a coherently illuminated light-field (diffuse glass) hologram and from the diffuse glass used in making the hologram.

(3) Theoretical calculations of the loci of intensity maxima and the intensity contrast due to diffraction from the edges of a square aperture as it combines with a reference plane wave at an angle. These calculations for a particular wavelength lead to the prediction of a dark-field hologram of a square aperture.

II. HOLOGRAPHIC INTERFEROMETRY

Work at TRW Systems

Heflinger, Wuerker, and Brooks[10-11] of TRW Systems have developed holographic techniques which are especially suitable for the analysis of fluid flow phenomena. Their work has been with both multiply exposed interferograms using a giant pulse laser[10] and holographically reconstructed

comparison beams using a continuous gas laser.[11] Application of these techniques has shown that (1) accurate alignment is not critical, (2) precision optical components are not required, (3) the technique may be used to observe either transient or stationary phenomena, and as has been mentioned, (4) three-dimensional interferograms are obtainable.

A Quantitative Test

In a quantitative test of such an interferogram of a conically-tipped 22 caliber bullet at Mach number 2.5, a good comparison was achieved with theoretical calculations which were made by assuming constant density behind the shock wave.[10] Actual density variation was known to be about 15 percent. A refined analysis of the predicted fringe pattern was made by Holds and Fuhs[12] taking into account the effect of variable density, and the results, when compared with the fringes of the TRW group's interferogram, verify the accuracy even more closely. The full impact of the advantages of this new technique are better appreciated when one examines existing interferometers.

The Mach-Zehnder Interferometer

The classical Mach-Zehnder interferometer is in use contemporarily in aeronautical test laboratories throughout the world. This system, developed in 1891, was a minor modification of the Jamin interferometer operated in 1865.[13] Its optical elements must be of the finest quality obtainable. The alignment of the four optical plates which compose the heart of the system must be accurate to within a fraction of a wavelength of light. Finally, the structure supporting such a system has generally

been of massive proportions to eliminate vibration. Recent work has been done on the use of light, heavily damped mounts;[14] however, most existing systems use the former mounting.

The Holographic Interferometer

Figure 1 is a schematic of a continuous reconstruction beam holographic interferometer. Note that the optical components of this system need consist of only two lenses and a prism. The quality of these components is not critical. A system such as this overcomes almost every drawback of the Mach-Zehnder interferometer and even challenges the much used Schlieren system for simplicity, since high quality optics are a factor in the latter. Production of a lightweight, inexpensive interferometer which is readily maintained and adjusted and, in addition, is suitable for wind tunnel use is certainly a desirable objective. The holographic interferometer makes such a device practicable.

The Holographic Interferometer at N.P.G.S.

The holographic interfermometer in use at the Naval Postgraduate School utilizes a Spectra-Physics Model 124 continuous wave helium-neon laser with a rated power output of 15 milliwatts at a wavelength of 6328 angstroms (visible red) as a coherent light source. A Spectra-Physics Model 331 collimating lens and spatial filter is used to expand the 1.1 millimeter diameter output beam of the laser to approximately 8.9 cm. Further beam expansion is accomplished using a double-concave lens with a negative 10 centimeter focal length and an 8-inch double-convex collimating lens. The resulting beam at the holographic plate is

approximately 15 cm in diameter, more than adequate to cover the 4 x 5 inch Kodak 649F spectroscopic plates used in the experiments. Early experiments were conducted satisfactorily with a 5 power microscope objective for initial beam expansion, and then the double concave lens.

A plexiglass prism is placed in the expanded output beam between the test section and the hologram in order to provide the reference beam. The prism dimensions are 4 x 6 inches, and the prism refracts one-half of the laser output beam by an angle of 10.5 degrees, thus providing for superposition of the test and reference beams at the holographic plate. An L-shaped aluminum plate holder was constructed so that the holograms can be exposed and returned precisely to their original position after developing. All components are mounted on a 10 foot long standard optical bench supported for structural rigidity by a 4 x 8 inch aluminum I beam. The entire apparatus rests at different times on a laboratory table or on several desks.

It should be noted that the optical components of the layout are not of top quality and have been chosen more for size and focal length than for any other feature. The prism, for instance, was cut from a block of plexiglass and hand polished. Using coherent light, optical quality is not a factor as long as optical path is duplicated. The Kodak 649F Spectroscopic Plates have an emulsion with extremely slow (ASA = .003), high resolution (2500 lines per millimeter) characteristics. The wavefront reconstruction capability of the plate lies in this high resolution with its ability to record an extremely fine diffraction pattern of the same order of magnitude as a wavelength of light.

Making the Holograms

Typical hologram sizes are 2 x 4 inches. Exposure time on the hologram is approximately 5 seconds with the beam expanded to give a uniform intensity for the 4 x 5 inch scene size. The plates are then developed in a high resolution plate developer for five minutes with a standard stop, fix, and rinse cycle.

Most holograms have been exposed at night both to obtain darkness for handling the plates and to reduce vibrations. If vibration does occur during exposure, the coherence of the light relative to the plate is destroyed, and the hologram is not formed. During exposures on the supersonic wind tunnel the interferometer is mounted on an insulated "floating" floor block designed for a Mach-Zehnder interferometer. No difficulty has been encountered with this setup. Successful holograms have been achieved with exposure times of up to thirty seconds.

Photography of the reconstructed scene is accomplished with a large diameter, 286 millimeter focal length lens and a Speed Graphic camera back. The focal plane shutter incorporated in the camera has an exposure capability of 1 millisecond. This speed is compatible with Polaroid ASA 3000 film. In certain cases too much light has been available, and has been attenuated with a single polarizing filter (possible because the laser beam is polarized.)

Dark Field Holograms

In the simple case illustrated in Figure 1 where the plane wave reference beam is unaltered prior to passage through the test area, the

resulting hologram is called dark field and is useful only in a two-dimensional sense. One may make interferometric analysis of heated bodies, flames, or the flow of compressible fluids in transparent channels. In the latter case the transparent channel must be present when the hologram is made. First attempts to record the interference patterns used only a film holder and shutter arrangement to capture the reconstructed real image. This projected beam, however, produced grossly inferior interferograms due to Fresnel diffraction fringes from the body and the shock waves. These diffraction phenomena created additional interference at the photographic plate. They were overcome entirely by focusing the reconstruction recording camera on the object creating the interference in the field.

The dark field technique was used on the 4 x 4 inch supersonic wind tunnel at the Postgraduate School to investigate the flow about a 40° cone model. While working with this arrangement it was found that a wide range of fringe orientation and spacing could be achieved. This was accomplished not only by rotating the prism and tilting the hologram, but also by moving the expanding or collimating lenses. Such flexibility of the system is valuable. For instance, the expanding lens could be moved within a range of 2 centimeters without losing the fringes. The movement of the prism and hologram were more critical. Micrometer adjustments on these components are planned in future installations.

Safety Considerations

Looking through the developed dark field hologram at the test scene is not only uncomfortable, for one is looking at the reconstructed laser source, but could cause permanent eye damage. Some safety experts have

placed the minimum amount of continuous incident optical power that can safely be sighted and focused by the eye at 1 microwatt for a wavelength of 6328A. Above that value there is a possibility of permanent retinal damage. To avoid the possibility of eye damage the collimated light through the test scene and hologram is allowed to project on a screen or directly on a photographic plate for recording interference patterns.

Typical Interferograms

Figure 2 shows two interferograms of the 40° cone at Mach 2.7. The upper half of the figure is an infinite fringe representation and includes the theoretical fringe prediction. The lower half of the figure is finite fringe to demonstrate that capability of the interferometer. High fringe contrast is to be noted and also the good agreement between predicted and actual fringes. The maximum relative error is less than three percent.

The interferometer performs very well in conjunction with the wind tunnel. Vibration problems have generally been easily overcome. The existing circular windows in the test section had greatly reduced the size of the scene available due to the necessity of passing the reference beam through the forward half of the window, but work has now been completed on plexiglass side windows which will open up the entire nozzle block. Interferometry through the plexiglass will be possible since optical quality is not critical. This will greatly increase the capability of this installation.

Figure 3 shows several finite fringe interferograms recorded through a hologram exposed to an open field which demonstrates the ease of making real time interferometric observations. The scenes were at atmospheric pressure and 70°F ambient. The size of the hologram was approximately 3 x 4 inches. The entire layout of the interferometer was the same as used on the wind tunnel with the test scene oriented in the area abeam of the prism.

Test subjects introduced into the field included a heated rod and plate to observe temperature gradients and convective effects in the air-flow about them. A match flame clearly showed the density distribution around itself. The microscope slide shows its deviation from optical flatness. The reduction of such finite fringe interferograms may be found in most complete texts on fluid flow or heat transfer.

The dark field method, using a continuous beam, is very suitable for wind tunnel and heat transfer studies. It has two other properties that also recommend its further development. It has sufficient intensity to make motion pictures of transient events, and the scene itself may be projected on a screen for instructional purposes.

Light Field Holograms

If a frosted glass plate is introduced into the test beam of the interferometer prior to the test area the resulting hologram will contain a completely three-dimensional reproduction of the scene. This is a light-field hologram. When it is replaced in the plate holder and reilluminated, both the original scene and the presently existing scene may be viewed

simultaneously through the hologram as a "window". The interference pattern of any difference between the two scenes will be three-dimensional in nature and may be viewed from various angles. Reference 10 contains excellent description and photographic evidence of the three-dimensional nature of the interferogram with a series of pictures taken at different angles. They show clearly how the interference pattern shifts as the visual reference is changed. Interferograms of this type suggest the possibility of solution of the three-dimensional flow fields about non-symmetric bodies that defy closed-form mathematical solutions. The light-field technique has no counterpart in current interferometry.

III. INTRODUCTORY ANALYSES

The Simple Hologram as a Diffraction Grating - Angles

To investigate whether or not a simple dark-field hologram behaves as a diffraction grating, a dark-field hologram with no test object present was exposed as shown in Figure 1. Reconstruction was accomplished utilizing the direct beam of the laser. The hologram was rotated about the horizontal axis (the axis parallel to the lines of the grating). The diffraction angle θ_d (measured from the 0 order) for orders $n = \pm 1$ and $n = 2$ were plotted as a function of the hologram rotation angle, θ_h. The results, were within experimental error of those predicted by classical diffraction grating theory[15] (see, for example, Figure 4 for $n = \pm 1$). This demonstrated that the ability of the simple dark-field hologram to diffract the incident beam into the various orders is similar to that

of the mechanically lined diffraction grating, in that simple diffraction grating theory correctly predicts the angles of the diffracted beams.

The Simple Hologram as a Diffraction Grating - Transmitted Amplitude

The angles of the diffracted beams for a simple dark field hologram behave according to the elementary grating theory. A natural question is whether or not the transmitted amplitude behaves according to that predicted by an elementary theory. Let the amplitude A_r and phase ψ of the reference beam be represented by

$$\tilde{E}_r = A_r e^{j(\omega t - \psi)} \tag{1}$$

where the phase angle ψ is

$$\psi = \frac{2\pi \sin \theta}{\lambda} y_p \tag{2}$$

the angle θ is defined in Figure 1. The geometry associated with y_p is illustrated by Figure 10. The object beam is represented by

$$\tilde{E}_o = A_o e^{j(\phi + \omega t)} \tag{3}$$

In equation (3), ϕ may be arbitrarily chosen as zero. The intensity of the light at the hologram is

$$I = (\tilde{E}_r + \tilde{E}_o)(\tilde{E}_r^* + \tilde{E}_o^*) \tag{4}$$

which reduces to

$$I = A_o^2 + A_r^2 + 2A_r A_o \cos \psi \tag{5}$$

If it is assumed that the film density is proportional to I then the transmitted amplitude will have a sinusoidal variation. For this case Givens[16] states that the amplitude in the zeroth beam should be proportional

to $A_r A_o$. In the higher order beams there should be zero amplitude.

A check was made with several dark field holograms to see whether the behavior was correctly predicted by the simple model. The intensity of +1 and -1 orders were not equal but varied by 10 to 20%. There was light diffracted into higher orders. The model did not correctly predict the intensities of the diffracted beams.

There are several reasons why the model is not adequate. The model assumes a linear relation between the resultant film density and the incident intensity at exposure. This is not the case due to threshold exposure. The emulsion of the film has a thickness which is not accounted for. Imperfections in the prism would cause a deviation from the plane wave of equation (1).

Intensity Variation Beyond the Light-Field Hologram and Diffuse Glass

Next, an investigation was made of the transmittance characteristics of a light field hologram and the ground glass plate, in terms of their intensity transmission functions. The theory of these is not offered here, but has been reported for the case of ground glass by Becherer and Ward[17]. Consider the reconstruction of a light-field hologram. A coherent laser beam of intensity $I_o(x,y)$ impinges on a diffuse glass plate as shown in Figure 5 and is modified in passage according to the transmission function T_d given by

$$T_d(x,y,\alpha) = \frac{\text{intensity at angle } \alpha}{\text{intensity at } (x,y)} \qquad (6)$$

That portion of the beam now at angle α next impinges upon the hologram at point (x',y') and is again modified by $T_h(x',y',\gamma)$ (defined in the

same manner as T_d except that γ represents the direction cosines to point (x",y")). The intensity of the pencil of rays arriving at point P via the path traced is

$$I_h(x",y") = I_o(x,y)\ T_d(x,y,\alpha)\ T_h(x',y',\alpha) \tag{7}$$

and the total intensity at P is the superposition of all such rays arriving at P.

First, a light-field hologram was constructed as shown in Figure 6, developed, returned, and reilluminated at incidence angles of 0^o, $\pm 10^o$, and $\pm 20^o$ (Figure 7). Relative intensity measurements were taken with an Eldorado Model 30 Differential Photometer, and results are shown in Figure 8.

Second, a ground glass plate was illuminated at 0^o incidence with a resulting intensity distribution as shown in Figure 9. The experimental data can be closely fitted by

$$T_d(\alpha) = e^{-8.0 \tan \alpha} \tag{8}$$

The Dark-Field Hologram of a Square Aperture

The dark-field hologram of a square aperture, as shown in Figure 10, is formed by the interference of the coherent plane wave reference beam, at angle θ, with the Fresnel diffraction pattern from the square aperture as both beams arrive at the hologram plate (plane 2).

The amplitude and phase of the reference beam at plane 2 may be described by the complex expression of equation (1). For good contrast on the developed hologram plate Givens [16] recommends that the reference beam be three times as bright as the scene beam, hence a factor of 3 is introduced. Discounting temporal variation, the phase of the electric vector of the reference beam is given by equation (2). For simplicity

of calculation, one may assume $\Psi = 0$ at $y_p = 0$, though it is in fact inconsequential.

The amplitude and phase of the light wave from the square aperture as it arrives at plane 2 may be obtained from the classical solution of the problem of diffraction from a square aperture which is treated in many texts on optics. The treatment given by Strong[18] is utilized here. The amplitude and phase of an incremental size wavelet emanating from an elemental area ds = dx dy at the aperture plane (plane 1) is described as a function of distance and angle by the Kirchoff Differential

$$\widetilde{dE}_p = \frac{jA_o}{r} \cos^2\left(\frac{\theta}{2}\right) e^{j\omega\left(t - \frac{r}{c}\right)} ds \qquad (9)$$

The derivation of this expression is described by Stone[19]. To apply the equation to our problem it is modified, integrated over the operture, and evaluated at plane 2. Note first that for typical dimensions, $\cos\frac{\theta}{2} \simeq 1$ and as regards amplitude, $r \simeq r_o$. Next use the Theorem of Pythagorus for r in the exponent, and expand the radical binomially, retaining only early terms:

$$r = \left[r_o^2 + (x_p - x_o)^2 + (y_p - y_o)^2\right]^{\frac{1}{2}} = r_o\left[1 + \tfrac{1}{2}\left(\frac{x_p - x_o}{r_o}\right)^2 + \tfrac{1}{2}\left(\frac{y_p - y_o}{r_o}\right)^2 + \ldots\right]$$

By using $j = e^{j\frac{\pi}{2}}$ and $\frac{\omega}{c} = \frac{2\pi}{\lambda}$, and by rearranging, one may express the integral as

$$\widetilde{E}_p = \left\{\frac{e^{j\frac{\pi}{4}}}{\lambda r_o}\int_{-x_o}^{+x_o} e^{-j\frac{\pi(x-x_p)^2}{\lambda r_o}} dx\right\}\left\{\frac{e^{j\frac{\pi}{4}}}{\lambda r_o}\int_{-y_o}^{+y_o} e^{-j\frac{\pi(y-y_p)^2}{\lambda r_o}} dy\right\}\left\{A_o e^{j\omega\left(t-\frac{r_o}{c}\right)}\right\} \qquad (10$$

where $e^{-j\frac{r_o}{c}}$ is an arbitrary phase shift and may be neglected. An alternate expression for $\tilde{E}_p$ is

$$\tilde{E}_p = \left\{\tilde{X}\right\}\left\{\tilde{Y}\right\}\left\{\tilde{Z}\right\} = A_o\, \tilde{X}\, \tilde{Y}\, e^{j\omega t}$$

By defining the variable

$$u^2 = \frac{2(x - x_p)^2}{\lambda\, r_o}\ ; \qquad du = \left(\frac{2}{\lambda r_o}\right)^{\frac{1}{2}} dx \tag{11}$$

and the limits

$$u_1 = u(+x_o, x_p)\ ; \qquad u_2 = u(-x_o, x_p)$$

one may put $\tilde{X}$ in the form

$$\tilde{X} = 2^{-\frac{1}{2}}\, e^{j\frac{\pi}{4}} \int_{u_1}^{u_2} e^{-j\frac{\pi}{2}u^2}\, du = 2^{-\frac{1}{2}}\, e^{j\frac{\pi}{4}} \left\{ \int_o^{u_2} e^{-j\frac{\pi}{2}u^2}\, du - \int_o^{u_1} e^{-j\frac{\pi}{2}u^2}\, du \right\} \tag{12}$$

The Fresnel Integrals are defined:

$$C(u) = \int_0^u \cos\left(\frac{\pi}{2}u^2\right) du \quad \text{and:} \quad S(u) = \int_0^u \sin\left(\frac{\pi}{2}u^2\right) du \tag{13}$$

so $$\tilde{X} = 2^{-\frac{1}{2}} e^{j\frac{\pi}{4}} \left\{ \left[C(u_2) - jS(u_2)\right] - \left[C(u_1) - jS(u_1)\right] \right\} = 2^{-\frac{1}{2}} e^{j\frac{\pi}{4}} \left[\Delta C_x - j\Delta S_x\right] \tag{14}$$

By defining $\Delta C_x \equiv C(u_2) - C(u_1)$, $A_x \equiv \left[\frac{1}{2}(\Delta C_x^{\,2} + \Delta S_x^{\,2})\right]^{\frac{1}{2}}$, and

$\phi_x \equiv \frac{\pi}{4} - \tan^{-1}\left(\frac{\Delta S_x}{\Delta C_x}\right)$ and making a similar analysis for $\tilde{Y}$ in terms of v, one can express $\tilde{X}$ and $\tilde{Y}$ in more convenient complex notation as follows:

$$\tilde{X} = \left[\tfrac{1}{2}(\Delta C_x^{\,2}+\Delta S_x^{\,2})\right]^{\frac{1}{2}} e^{j(\frac{\pi}{4}-\tan^{-1}\frac{\Delta S_x}{\Delta C_x})} \equiv A_x\, e^{j\phi_x}$$

$$\tilde{Y} = \left[\tfrac{1}{2}(\Delta C_y^{\,2}+\Delta S_y^{\,2})\right]^{\frac{1}{2}} e^{j(\frac{\pi}{4}-\tan^{-1}\frac{\Delta S_y}{\Delta C_y})} \equiv A_y\, e^{j\phi_y} \qquad (15)$$

Fresnel's Integrals are tabulated in many mathematical tables, e.g. Jahnke - Emde - Losh[20]. Cornu's Spiral, available in most optics texts (e.g. Jenkins and White[15], Strong[18], Stone[19]) provides a convenient solution for ΔC_x and ΔS_x. The total amplitude and phase may thus be expressed as

$$A_p = A_o A_x A_y \quad \text{and} \quad \phi = \phi_x + \phi_y$$

As in the case of a simple hologram, the amplitude and phase of the resulting wavefront at plane 2 is the sum of the two; $\tilde{E}_t = \tilde{E}_r + \tilde{E}_p$, and the intensity will be

$$\begin{aligned} I = \tilde{E}_t\tilde{E}_t^{\,*} &= (A_r e^{j\Psi} + A_p e^{j\phi})(A_r e^{-j\Psi} + A_p e^{-j\phi}) \\ &= A_r^{\,2} + A_p^{\,2} + 2A_rA_p\cos(\phi - \Psi) \end{aligned} \qquad (16)$$

which has maximum values of $(A_r + A_p)^2$ at $(\phi - \psi) = 2n\pi$ and minimum values of $(A_r - A_p)^2$ at $(\phi - \Psi) = (2n - 1)\pi$. Thus regions of maximum intensity will form the dark lines of the intricate diffraction grating which is a hologram.

To provide perspective at this point, sample calculations have been completed. Consider the dimensions:

$r_o = 12.642$ cm

$x_o = y_o = 1.0$ cm

$\lambda = 6328\text{Å} = 6.328 \cdot 10^{-5}$ cm

$\theta = 0.1582$ ($\sin \theta = 0.1582$)

which yield: $u = 50(1.0 - x_p)$, $v = 50(1.0 - y_p)$, and $\Psi = 2\pi(2.5 \cdot 10^3)y$. Values of u_2 and ϕ_x are tabulated versus x_p in Table I. Values of v, ϕ_y and y are exactly the same. Notice that if the test beam were an unaltered plane wave, the interference at the hologram plate would produce a lined diffraction grating of 2500 lines per centimeter. These lines would correspond to the position of the plate where $\Psi = 2n\pi$ and do provide good reference positions for the calculations. The integer n can be arbitrarily assigned a value of 0.

Darkening occurs where $\phi - \Psi = 2n\pi = 0$, or where $\phi = \Psi$. In region A, y is close to zero, v_1 is about -50, near the negative eye of Cornu's Spiral, and v_2 is correspondingly near +50. Therefore ϕ_y remains very close to zero throughout the region, and $\phi \simeq \phi_x$. As x_p varies from 0 to greater than 1 cm, one finds ϕ_x oscillating about zero with slowly increasing amplitude as x approaches the edge (1 cm) and u_2 approaches zero. Therefore to plot the region of $\phi = \Psi$, one need only plot ϕ_x on the same scale as Ψ. The ϕ_x curves correspond exactly to the darkened lines of the film. This is shown on Figure 11. For region B, $\phi_x = 0$; consequently one plots both Ψ and ϕ_y on the same scale, as shown in Figure 12. Where the curves cross (slightly more than 2500 times per centimeter) will give the position of the almost straight grating lines.

TABLE I

PHASE OF THE APERTURE BEAM AT THE HOLOGRAM PLATE

x (y)	u_2 (v_2)	ϕ_x (ϕ_y)	x (y)	u_2 (v_2)	ϕ_x (ϕ_y)
.998	0.1	5.2°	1.002	-0.1	-6.2°
.996	0.2	9.2°	1.004	-0.2	-13.8°
.994	0.3	12.2°	1.006	-0.3	-22.6°
.992	0.4	14.3°	1.008	-0.4	-33.3°
.990	0.5	15.8°	1.010	-0.5	-45.0°
.988	0.6	16.0°	1.012	-0.6	-57.0°
.986	0.7	14.9°	1.014	-0.7	-71.0°
.984	0.8	13.5°	1.016	-0.8	-86.9°
.982	0.9	11.4°	1.018	-0.9	-103.8°
.980	1.0	8.7°	1.020	-1.0	-122.6°
.978	1.1	6.6°	1.022	-1.1	-142.9°
.976	1.2	2.2°	1.024	-1.2	-164.8°
.974	1.3	-1.2°	1.026	-1.3	-184.4°
.972	1.4	-4.2°	1.028	-1.4	-213.6°
.970	1.5	-6.7°	1.030	-1.5	-240.5°
.968	1.6	-7.7°	1.032	-1.6	-269.0°
.966	1.7	-6.8°	1.034	-1.7	-299.4°
.964	1.8	-3.8°	1.036	-1.8	-331.4°
.962	1.9	0.6°	1.038	-1.9	-365.2°

Region C is determined by a combination of the two methods. At $x = 1.0$ cm (the edge), $\phi_x = 0$ so the vertical spacing of the dark lines is the same as region B. Using these points as positions of $(\phi_y - \psi) = 0$ one repeats the procedure for region A with a modified vertical scale. The assumption of linear variation over each cycle of ψ will introduce only very small distortion in the curves. Figure 13 is an exaggerated sketch of the three areas and the predicted form of the diffraction grating with only a very few lines represented.

Contrast between light and dark lines on the film according to the usual definition is given by:

$$\text{Contrast} = D = \frac{I_{max} - I_{min}}{I_{max} + I_{min}} = \frac{(A_r + A_p)^2 - (A_r - A_p)^2}{(A_r + A_p)^2 + (A_r - A_p)^2} = \frac{6A_xA_y}{(A_xA_y)^2 + 9} \qquad (17)$$

Contrast is shown on Figure 14 as a function of u_2 for region A, B, and the line of equal x and y across region C. The sketch of Figure 13 utilizes line thickness to illustrate the effect of contrast upon the plate.

IV. CONCLUSION

Experience gained so far with the continuous beam holographic interferometer indicates that it is very well suited for experimental work in compressible fluid flow investigations. It overcomes the drawbacks of the Mach-Zehnder interferometer and decreases the difficulty of interferometry. The mechanics of the technique are only slightly more complex than those involved in obtaining shadowgraphs.

That optical quality and alignment are non-critical has been adequately substantiated. Hand-made plastic prisms and use of ground glass prove the former, and manual adjustment of the lenses, prism, and hologram bear out the latter. The light weight and potential of high mobility of the system make it ideal for laboratories where many different projects may use interferometric analysis in their studies.

The quantitative capability of the technique in the classical two-dimensional sense has been amply proven with very accurate fringe prediction of the 0.22 caliber bullet[10] and the good agreement between the 40° cone prediction and the interferogram. (See Figure 2).

While not in themselves conclusive, the experiments with dark and light-field holograms are worthy of note, in that they show that while a simple dark-field hologram does behave as a mechanically lined diffraction grating as has been predicted, the amplitude distribution as a function of angle of a typical dark or light-field hologram is not so predictable.

Knowledge of the intensity beyond a ground glass plate must necessarily be a part of any analysis of a three-dimensional interferogram. One of the key, unsolved problems of holographic interferometry is to relate the three-dimensional interferogram to a three-dimensional density distribution. Some preliminary experiments were conducted aimed at gaining insight to this unsolved problem. A dark-field hologram was examined to ascertain whether or not elementary theory would adequately predict the diffracted beams. Angles are correctly predicted; intensities are not correctly determined by an elementary theory. A

three-dimensional interferogram requires use of a diffuse glass plate in the scene beam. Intensity distribution from diffuse glass plates and from light field holograms were studied experimentally. Intensity distribution arising from light-field holograms showed an anomolous peak; see Figure 8.

It is felt that the complete prediction of a dark-field hologram from basic theory is extremely instructive and develops intuition relative to the holographic process. As such it should be of interest to anyone who desires to master the field. The prediction is complete yet remains close to the physics of holography. The oft-used methods of communications theory are somewhat more removed.

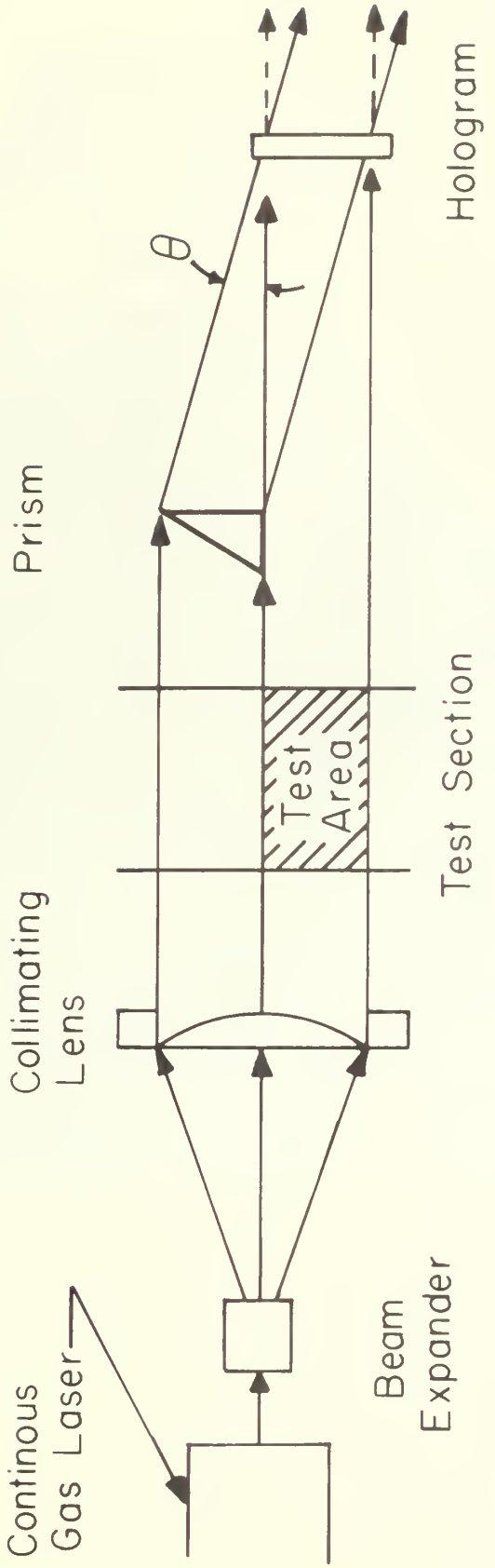

Fig. 1 The Holographic Interferometer

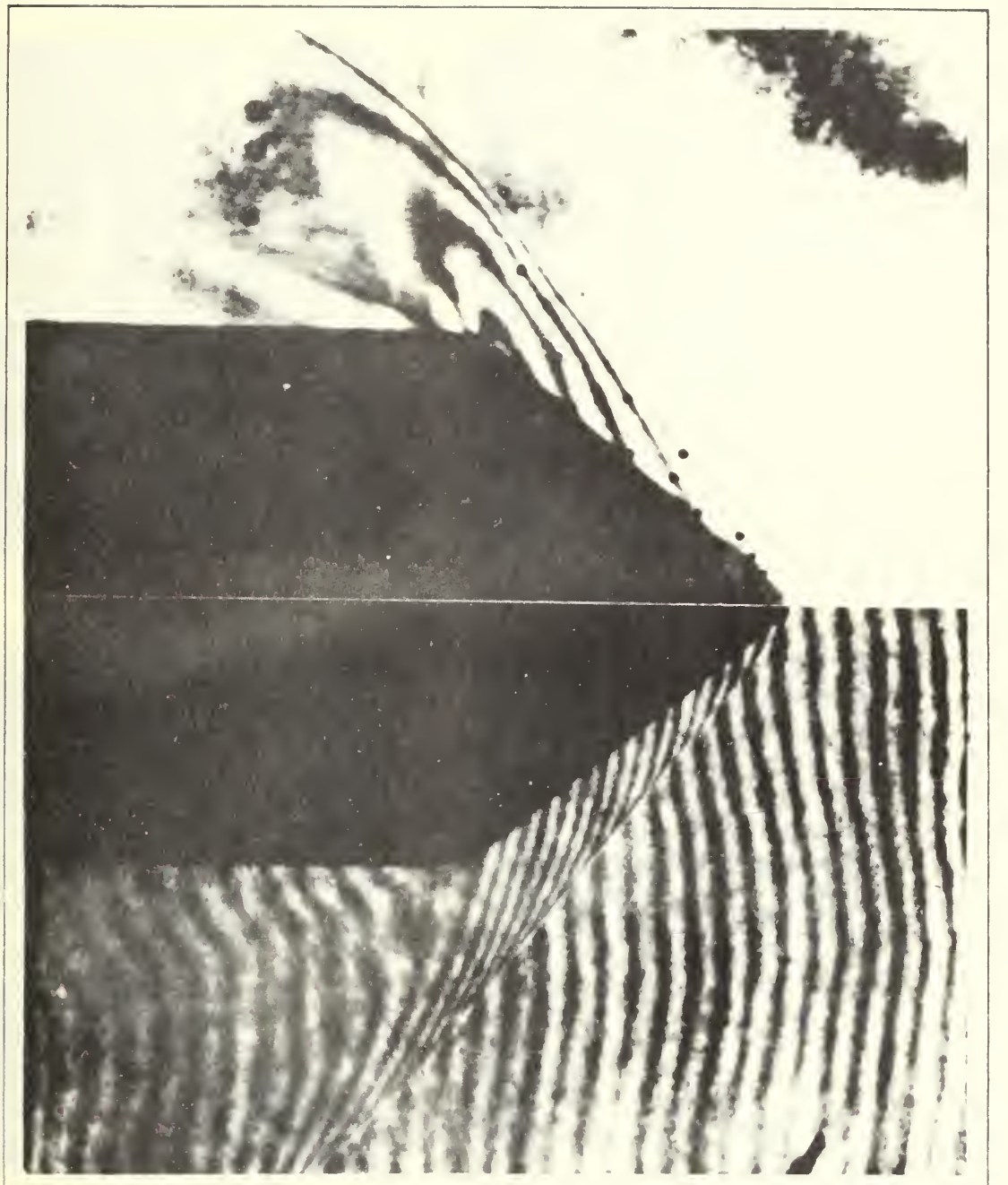

INTERFEROGRAM OF 40° CONE AT MACH 2.7;
INFINITE AND FINITE FRINGE.
DOTS REPRESENT VARIABLE DENSITY
SOLUTION OF FRINGE PREDICTION.

Fig. 2

HEATED ROD

HEATED PLATE

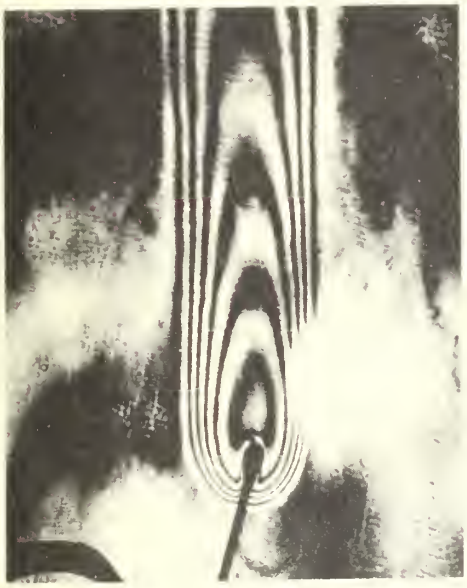

FLAME

SLIDE GLASS

Fig. 3 DARK FIELD INTERFEROGRAMS OF VARIOUS SUBJECTS

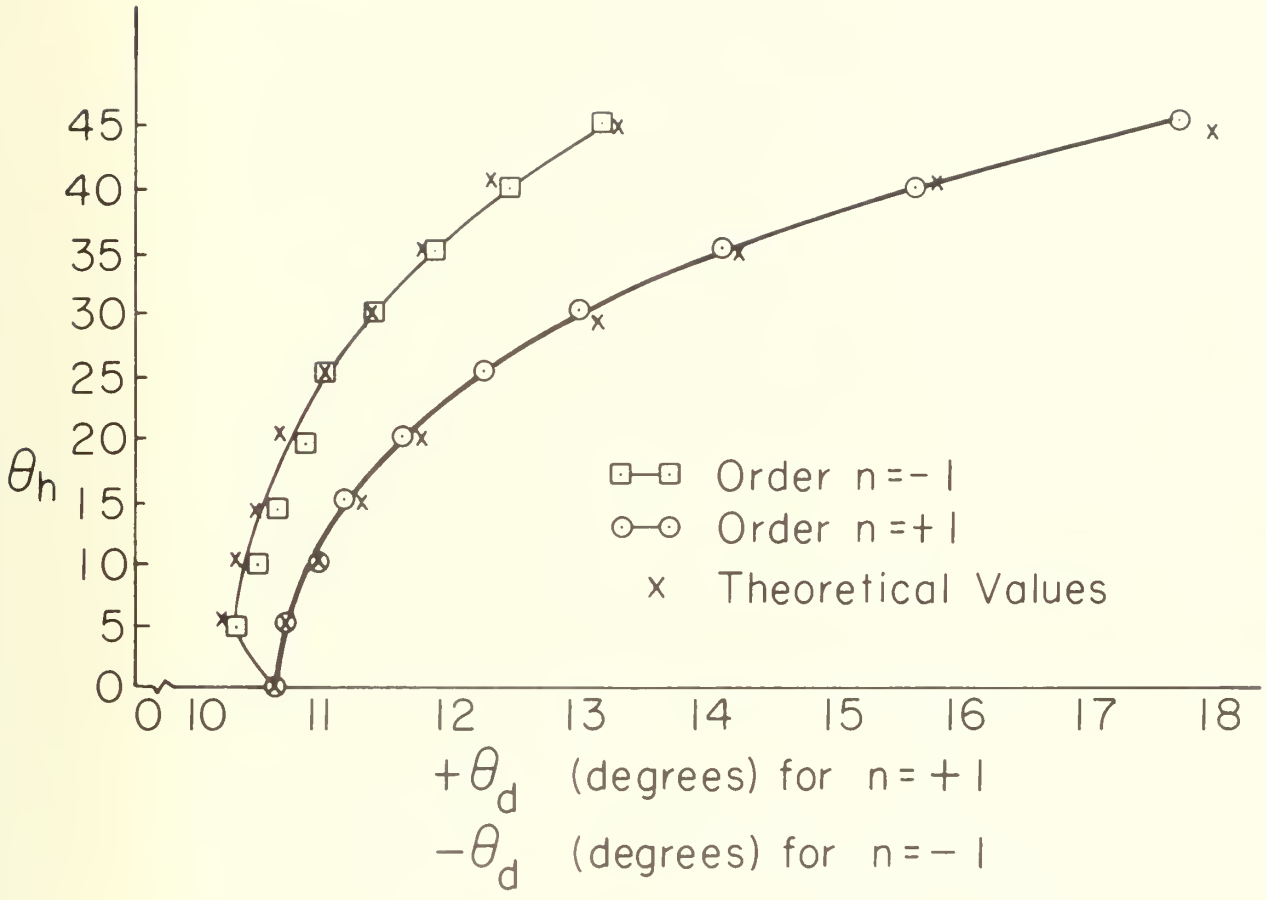

Fig. 4 The Hologram as a Diffraction Grating.
Diffraction angle θ_d vs. Incidence Angle.

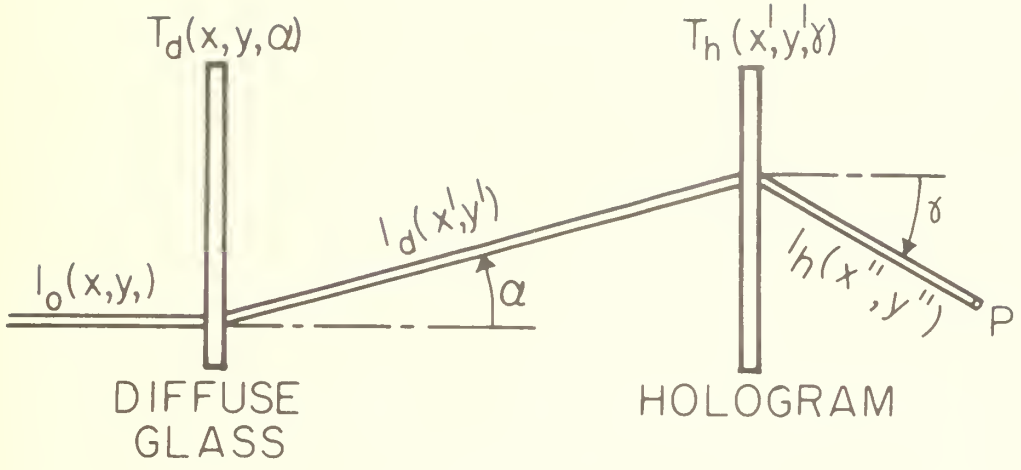

Fig. 5 Geometry for the Light Field Hologram Intensity Problem

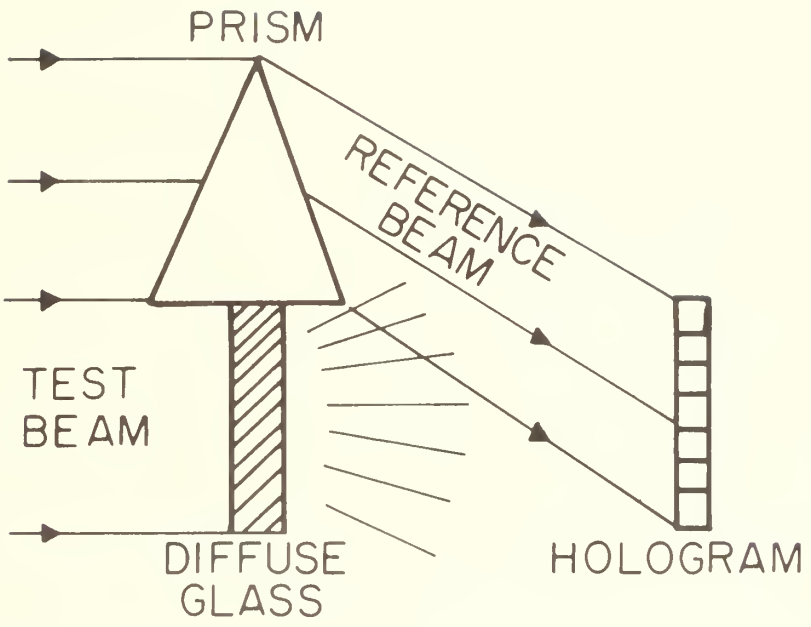

Fig. 6 Making a Light Field Hologram

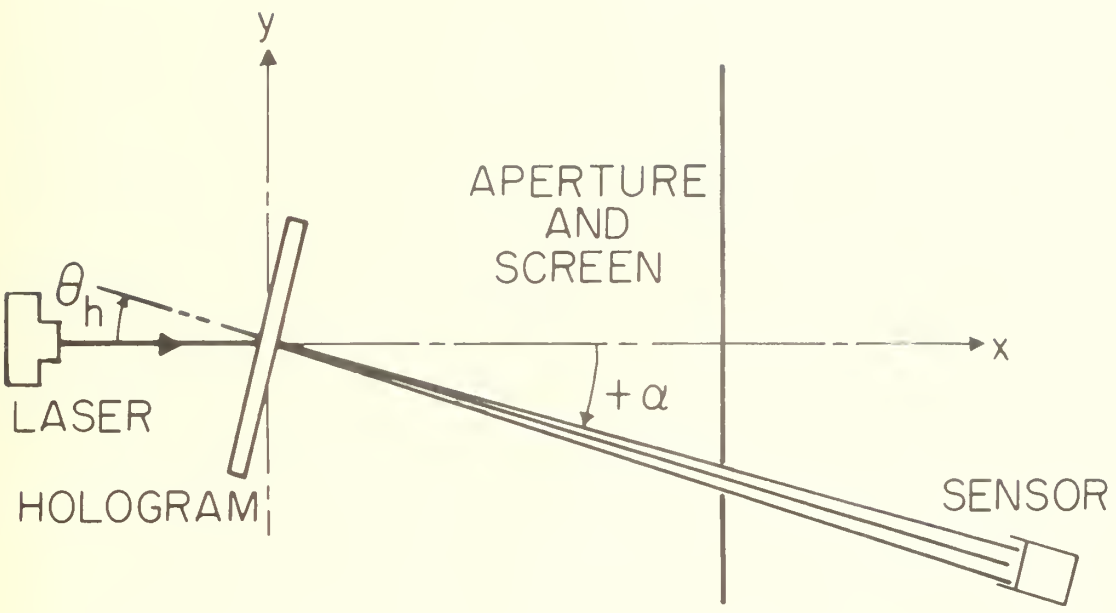

Fig. 7 Intensity Detection beyond a Hologram

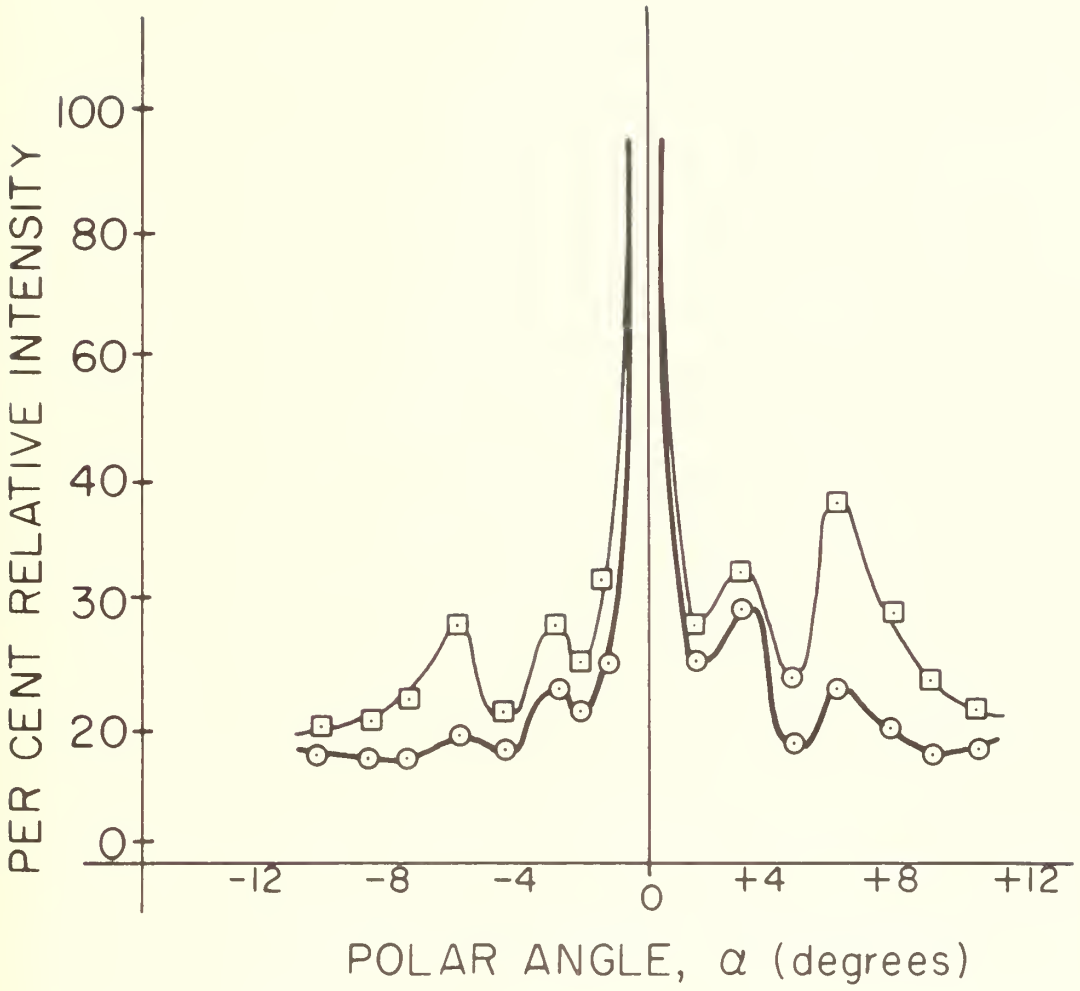

Fig. 8 Typical Relative Intensity vs. Polar Angle beyond a Diffuse Glass Hologram

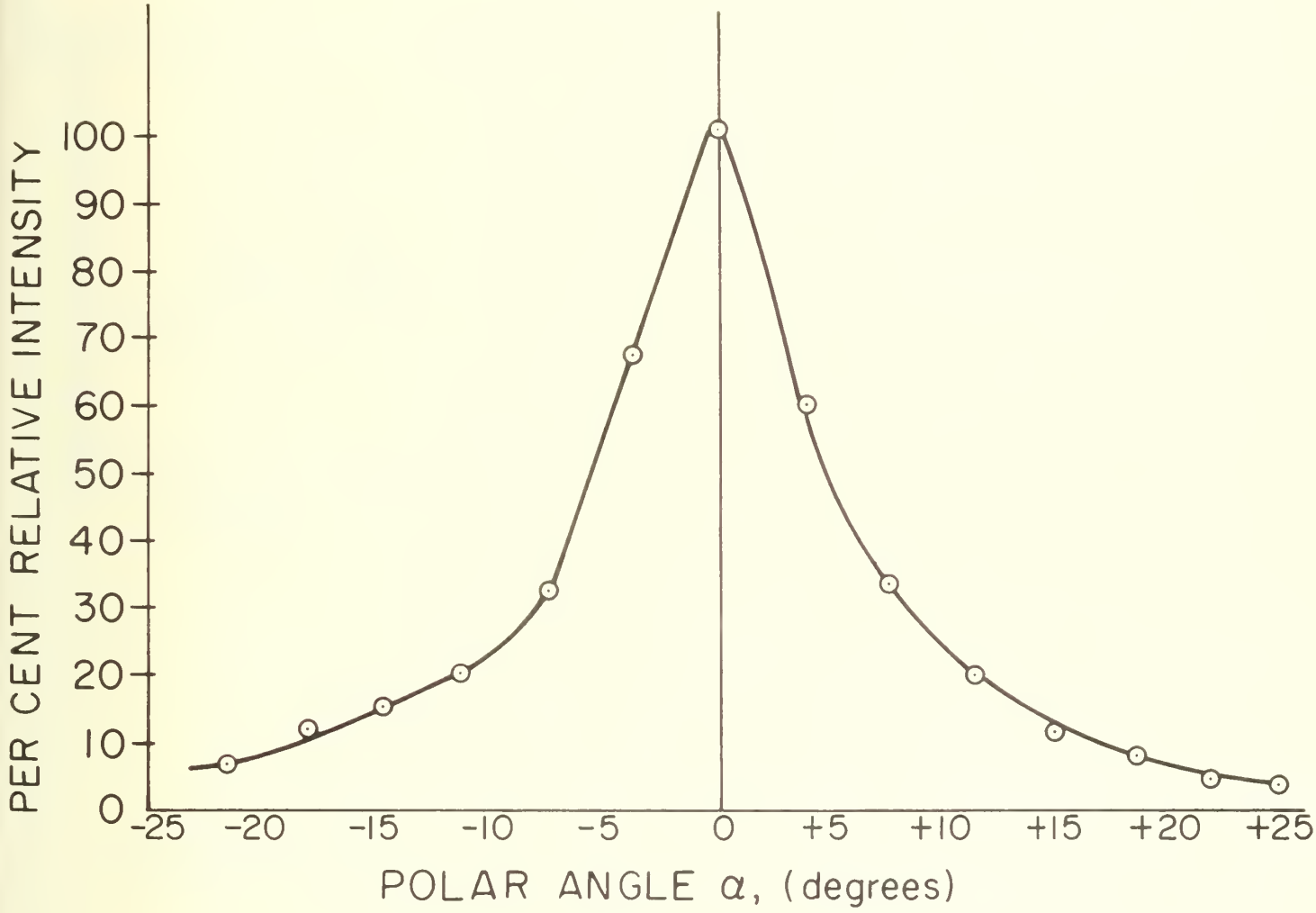

Fig. 9 Relative Intensity vs. Polar Angle beyond a Ground Glass Plate

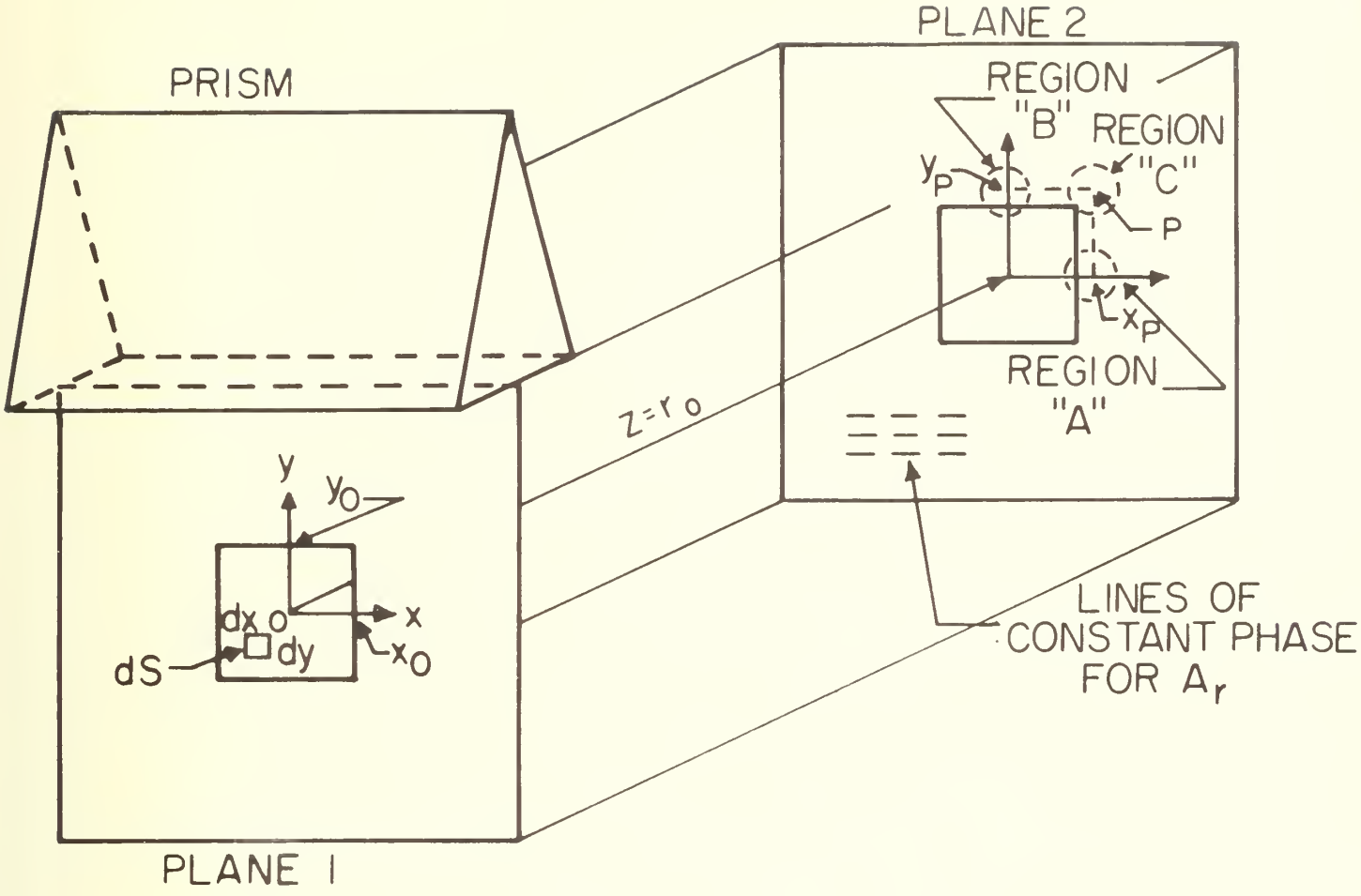

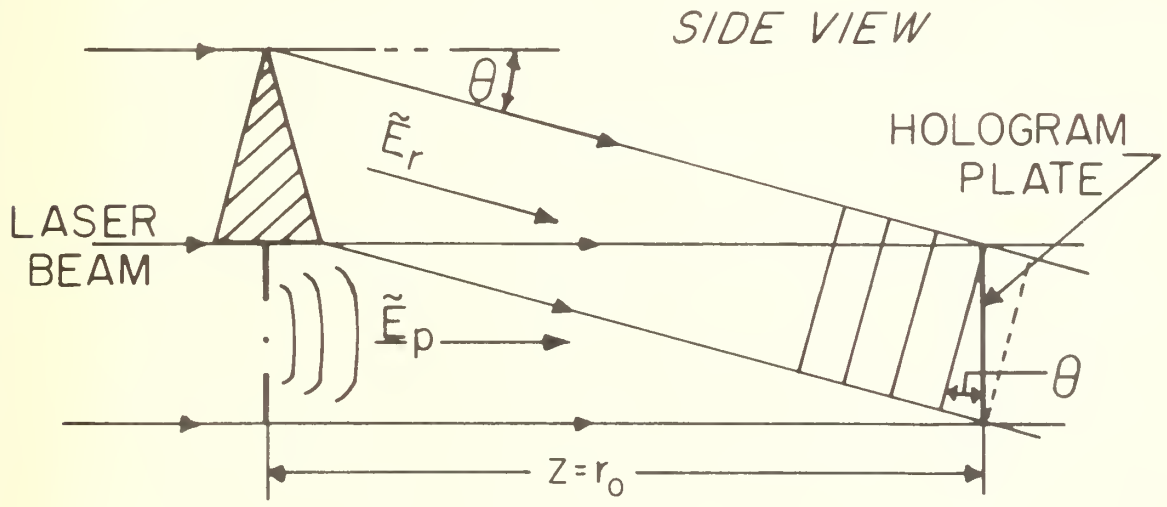

Fig. 10 Geometry of the Hologram Problem

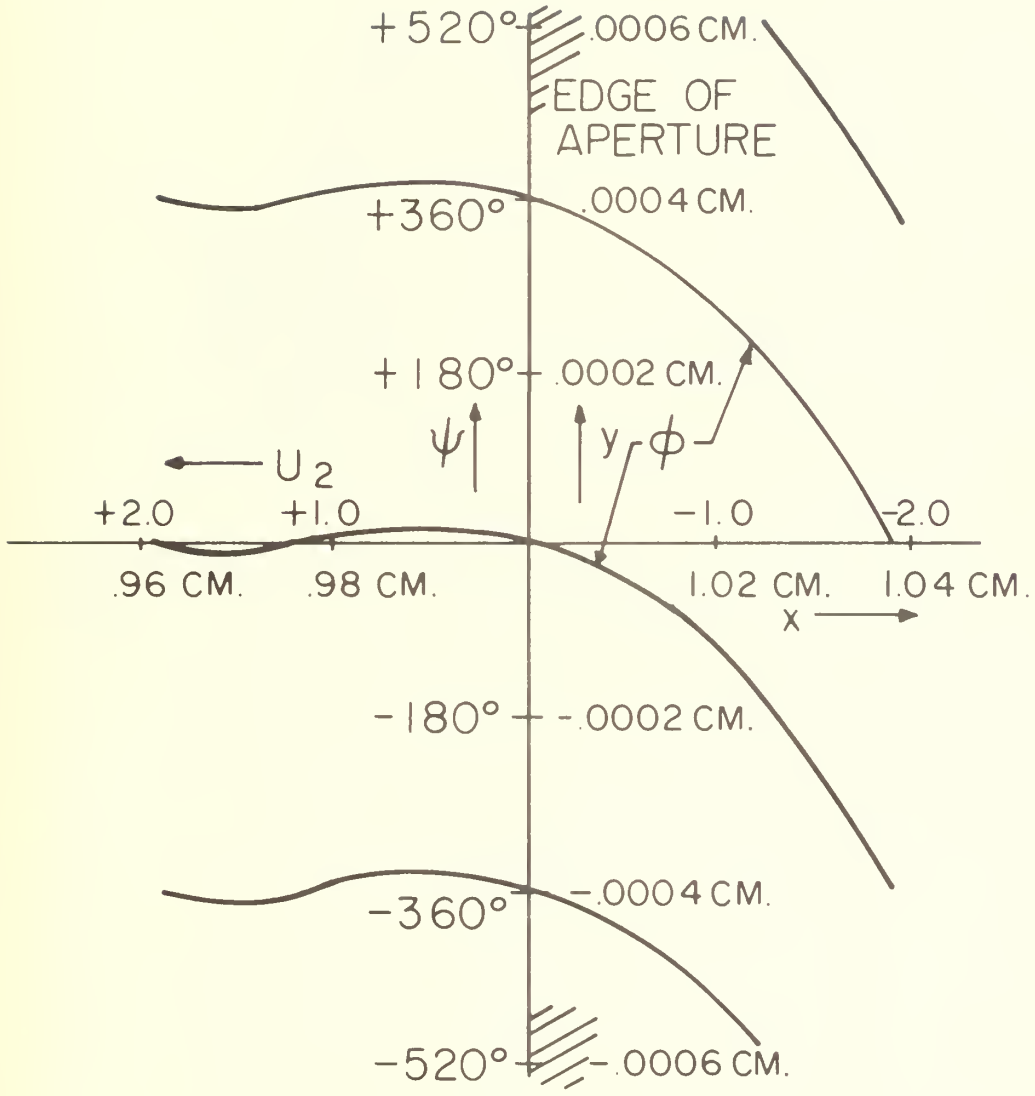

Fig. 11 Hologram Dark Lines corresponding to Positions of equals ∅ for Region "A"

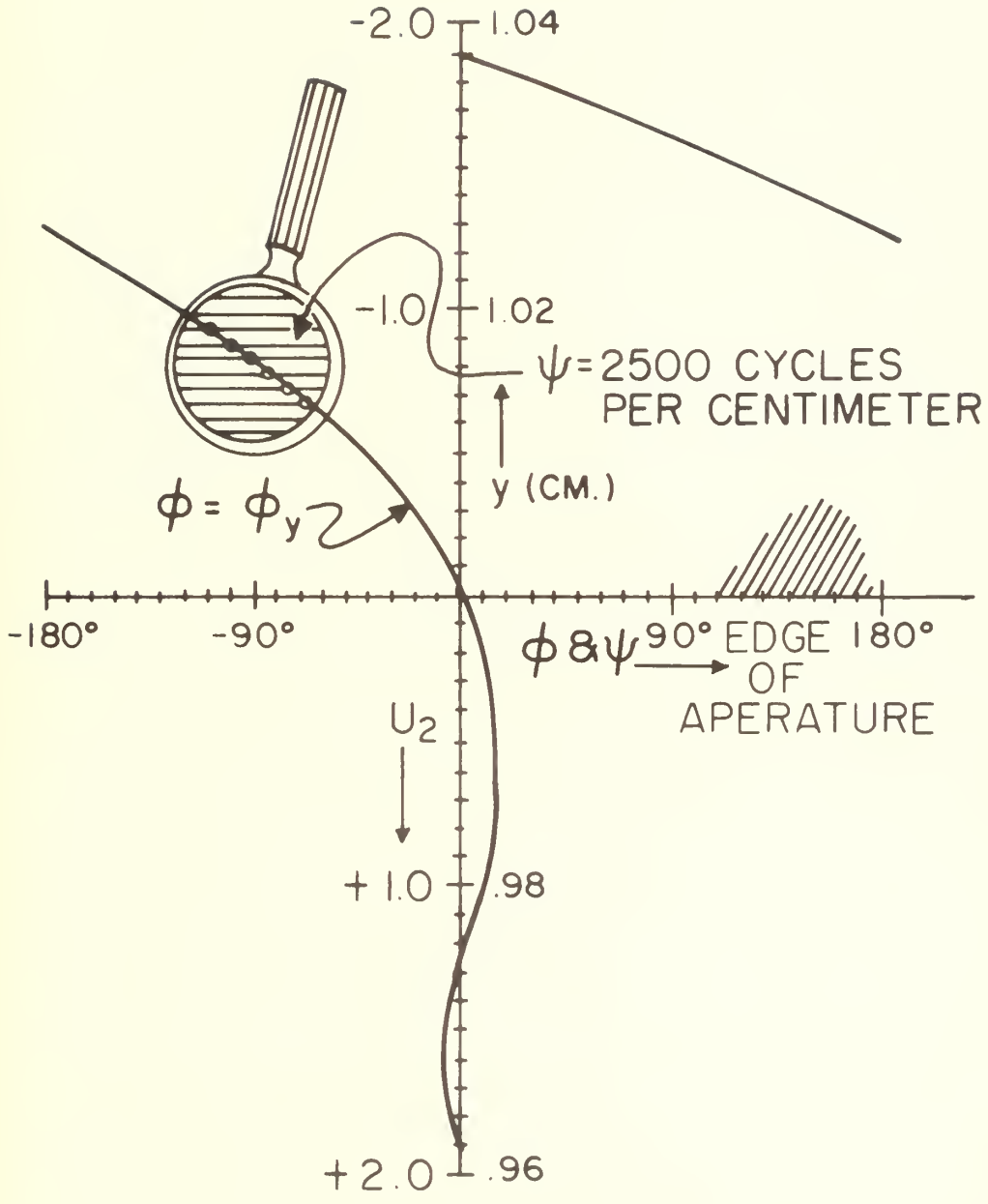

Fig. 12 Location of Hologram Dark Lines corresponding to Positions of equals ∅ for Region "B"

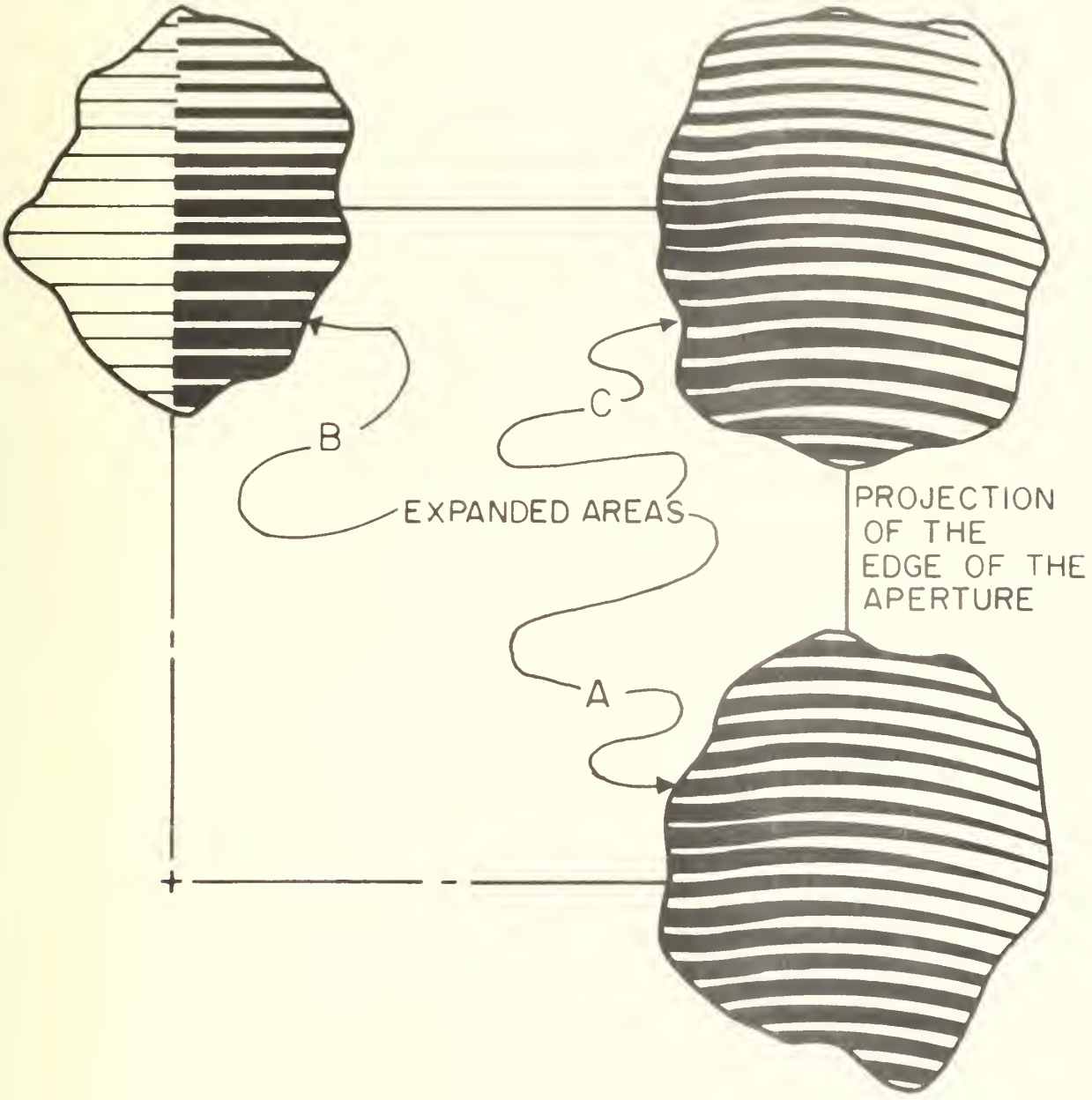

Fig. 13 Sketch of Predicted Hologram Patterns for Regions "A", "B" and "C"

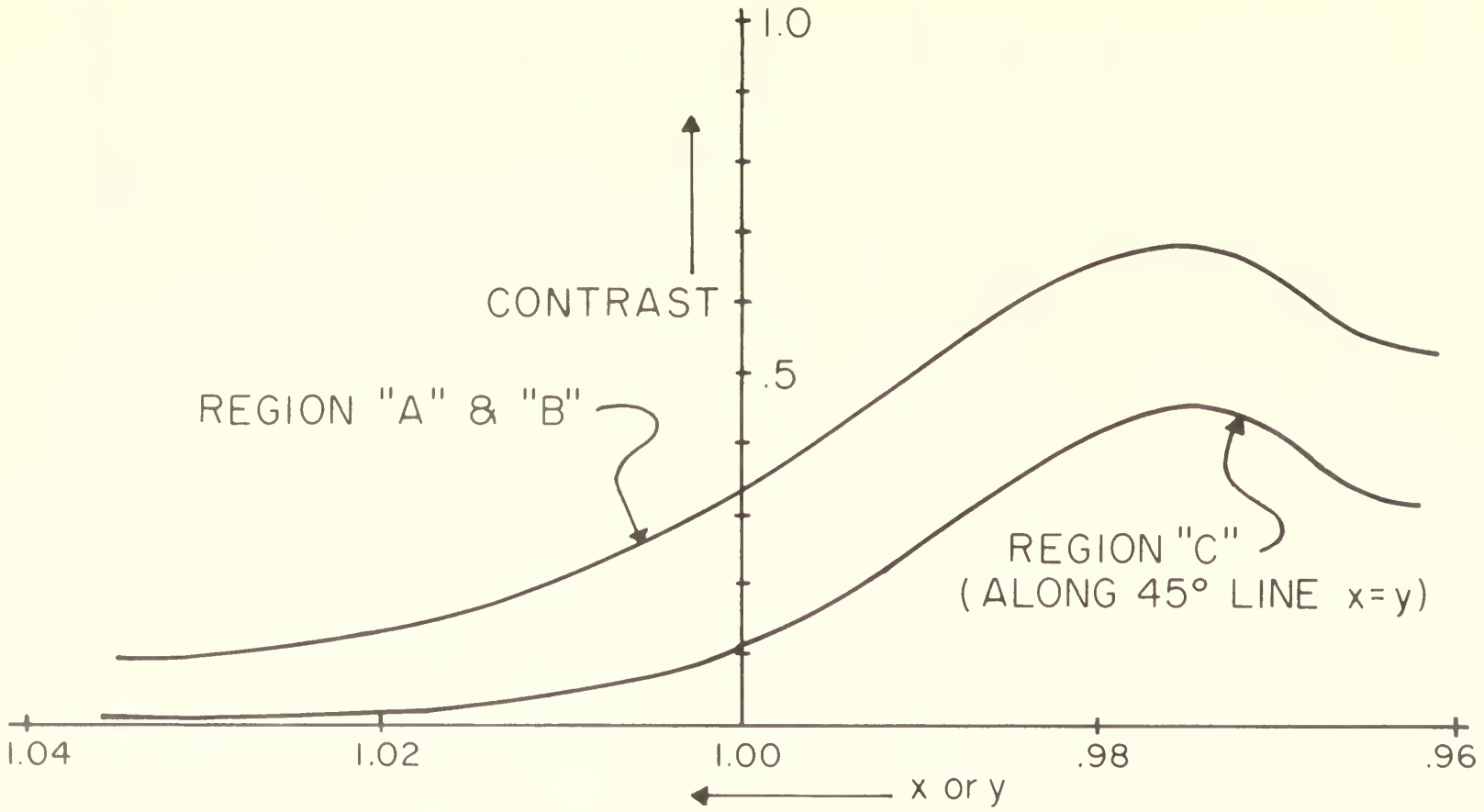

Fig. 14 Contrast on the Hologram

REFERENCES

1. Gabor, D., "A New Microscopic Principle," Nature, 161, May, 1948, pp. 777-778.

2. Gabor, D., "Microscopy by Reconstructed Wavefronts," Proceedings of The Royal Society, London, A197, 1949, pp. 454-487.

3. Leith, E. N., and Upatnieks, J., "Photography by Laser," Scientific American, Vol. 212, No. 6, June, 1965, pp. 24-35.

4. Pennington, K. S., "Advances in Holography," Scientific American, Vol. 218, No. 2, February, 1968, pp. 40-48.

5. Brandt, G. B., "Techniques and Applications of Holography," Electro-Technology, April, 1968, pp. 53-72.

6. Leith, E. N., and Upatnieks, J., "Reconstructed Wavefronts and Communications Theory," J. Opt. Soc. of Amer., Vol. 52, No. 10, October, 1962, pp. 1123-1130; "Wavefront Reconstruction with Continuous Tone Objects," J. Opt. Soc. of Amer., Vol. 53, No. 12, December, 1963, pp. 1377-1381; "Wavefront Reconstruction with Diffused Illumination and Three-Dimensional Objects," J. Opt. Soc. of Amer., Vol. 54, No. 11, November, 1964, pp. 1295-1301.

7. DeVelis, J. B., and Reynolds, G. O., Theory and Applications of Holography, Addison-Wesley Publishing Co., Reading, Mass., 1967.

8. Stroke, G. W., An Introduction to Coherent Optics and Holography, Academic Press, Inc., New York, 1966.

9. Chambers, R. P., and Courtney-Pratt, J. S., "Bibliography on Holograms," Journal of the SMPTE, Vol. 75, April, 1966, pp. 373-435; "Bibliography on Holograms - II," Journal of the SMPTE, Vol. 75, August, 1966, pp. 759-809; "Bibliography on Holograms - III," Journal of the SMPTE, Vol. 76, pp. 392-395.

10. Heflinger, L. O., Wuerker, R. F., and Brooks, R. E., "Holographic Interferometry," Journal of Applied Physics, Vol. 37, No. 2, February, 1966, pp. 642-649.

11. Brooks, R. E., Heflinger, L. O., and Wuerker, R. F., "Interferometry with a Holographically Reconstructed Comparison Beam," Applied Physics Letters, Vol. 7, No. 9, 1 November 1965, pp. 248-249.

12. Holds, J. H., "Aeronautical Applications of Holographic Interferometry," M. S. Thesis, Department of Aeronautics, Naval Postgraduate School, Monterey, California, June, 1967; Holds, J. H., and Fuhs, A. E., "A Refined Analysis of a Holographic Interferogram," Journal of Applied Physics, Vol. 38, No. 13, December, 1967, pp. 5408-5409.

13. Tolansky, S., An Introduction to Interferometry, Longmans, Green, and Co., New York, 1955, P. 115.

14. Ashkenas, H. I., and Bryson, A. E., "Design and Performance of Simple Interferometer for Wind-Tunnel Measurements," Journal of Aeronautical Sciences, Vol. 18, 1951, p. 82.

15. Jenkins, F. A., and White, H. E., Fundamentals of Optics, 3rd ed., McGraw-Hill Book Co., New York, 1957, p. 333.

16. Givens, M. P., "Introduction to Holography," Journal of Applied Physics, Vol. 35, November, 1967, pp. 1056-1064.

17. Becherer, R. J., and Ward, J. H., "Scattering of Laser Radiation by Ground Glass," presented at the 1966 Annual Meeting of the Optical Society of America, 19 October 1966.

18. Strong, J., Concepts of Classical Optics, W. H. Freeman and Co., San Francisco, 1958, Chapt. IX.

19. Stone, J. M., Radiation and Optics, McGraw-Hill Book Co., New York, 1963, Chapt. 10.

20. Jahnke - Emde - Losch, Tables of Higher Functions, Sixth Edition, McGraw-Hill Book Co., New York, 1960, pp. 34-35.

INITIAL DISTRIBUTION LIST

		No. Copies
1.	Defense Documentation Center Cameron Station Alexandria, Virginia 22314	20
2.	Library Naval Postgraduate School Monterey, California	2
3.	Commander, Naval Air Systems Command Navy Department Washington, D. C. 20360	1
4.	Dr. A. E. Fuhs Aero Propulsion Lab Wright Patterson AFB, Ohio 45433	1
5.	Chairman, Department of Aeronautics Naval Postgraduate School Monterey, California	1
6.	Ensign J. G. Sullivan, USN 16121 Northfield Street Pacific Palisades, California 90272	3
7.	Dr. L. O. Heflinger TRW Systems 1 Spacepark Avenue Redondo Beach, California 90278	1
8.	Dr. E. S. Lamar Chief Scientist Naval Air Systems Command Navy Department Washington, D. C. 20360	1
9.	Professor D. J. Collins Department of Aeronautics Naval Postgraduate School Monterey, California	1
10.	Lt. J.H. Holds, USN 21 W. Goguac Street Battle Creek, Michigan 49015	1

11. Mr. K. G. Orman — 1
Command Control and Guidance Administrator (Code 360)
Research and Technology
Naval Air Systems Command
Washington, D. C. 20360

12. Mr. I. H. Gatzke — 1
Surveillance Administrator (Code 370)
Naval Air Systems Command
Navy Department
Washington, D. C. 20360

13. LT R. D. Matulka, USN — 3
Department of Aeronautics
Naval Postgraduate School
Monterey, California

14. Central Files — 1
Naval Postgraduate School
Monterey, California

15. Dean of Research Administration — 2
Naval Postgraduate School
Monterey, California

UNCLASSIFIED

Security Classification

DOCUMENT CONTROL DATA - R & D

(Security classification of title, body of abstract and indexing annotation must be entered when the overall report is classified)

1 ORIGINATING ACTIVITY (Corporate author)	2a. REPORT SECURITY CLASSIFICATION
Naval Postgraduate School Monterey, California 93940	Unclassified
	2b. GROUP

3 REPORT TITLE

AERONAUTICAL APPLICATIONS OF HOLOGRAPHIC INTERFEROMETRY

4 DESCRIPTIVE NOTES (Type of report and, inclusive dates)

Technical Report

5 AUTHOR(S) (First name, middle initial, last name)

MATULKA, R. D., LT, USN; HOLDS, J. H., LT, USN; SULLIVAN, J. G., ENS, USN and FUHS, A. E.

6 REPORT DATE	7a. TOTAL NO. OF PAGES	7b. NO. OF REFS

8a. CONTRACT OR GRANT NO.	9a. ORIGINATOR'S REPORT NUMBER(S)
b. PROJECT NO.	NPS-57FU8101A
c.	9b. OTHER REPORT NO(S) (Any other numbers that may be assigned this report)
d.	

10 DISTRIBUTION STATEMENT

This document has been approved for public release and sale; its distribution is unlimited.

11. SUPPLEMENTARY NOTES	12. SPONSORING MILITARY ACTIVITY

13. ABSTRACT

The use of holography for the production of wind-tunnel interferograms of the Mach-Zehnder type is described with a discussion of the possibility of extending the process toward the interferometric study of three-dimensional flow fields. Two initial studies toward an understanding of the processes involved in three-dimensional interferometric reduction are described: (1) the hologram as a diffraction grating, and (2) intensity variation beyond both a hologram and a diffuse glass plate. Lastly, a complete prediction of a hologram of a simple, two dimensional, aperture is made. This prediction provides a tutorial device for the understanding of holography of the type used in holographic interferometry.

DD FORM 1 NOV 68 1473 (PAGE 1)

S/N 0101-807-6811

UNCLASSIFIED

Security Classification

A-31408

14 KEY WORDS	LINK A		LINK B		LINK C	
	ROLE	WT	ROLE	WT	ROLE	WT
HOLOGRAPHY OPTICS						
WAVEFRONT RECONSTRUCTION						
ELECTRO-OPTICS						
INTERFEROMETRY						
GAS DYNAMICS						